Optik - International Journal for Light and Electron Optics 332 (2025) 172350

Contents lists available at ScienceDirect

Optik - International Journal for Light and Electron Optics

journal homepage: www.elsevier.com/locate/ijleo

Original research article

Method to identify optical path transmittance by using cat's-eye retroreflectors

Hiroki Natsume [a,*], Sin-iti Kitazawa [b], Kunpei Nojiri [b], Kazuhiro Torimoto [b], Eiichi Yatsuka [b], Tomohiro Yokozuka [b], Takanori Kikuchi [b], Yoshihiko Nunoya [b]

[a] Global Research Institute of Nuclear Energy, Tokai University, Hiratsuka, 259-1207, Japan
[b] Naka Fusion Institute, National Institutes for Quantum Science and Technology, Naka, 311-0193, Japan

ARTICLE INFO

Keywords:
Retroreflector
Reflectance
Sensitivity calibration
Cat's eye
Optical diagnostic

ABSTRACT

In optical systems used in nuclear fusion reactors, the reflectance of in-vessel mirrors may change due to the deposition of impurities or corrosion. To address this issue, a methodology was proposed whereby ex-vessel light is used to determine the transmittance of an optical system by measuring the light reflected by a retroreflector that is temporarily placed at the tip of the optical system. However, because the reflectance of retroreflectors themselves is not always constant, a reliable method for absolute sensitivity calibration has yet to be established. In this study, we developed a method for measuring the reflectance of a cat's-eye retroreflector and, consequently, the transmittance of the desired optical system. Developing this method entailed an analysis of the variation in number of reflections and reflection positions within the cat's-eye retroreflector.

1. Introduction

A retroreflector is a device designed to reflect incident light back towards its source, in a direction parallel to the incoming light, regardless of the angle of incidence. Historically, retroreflectors have constituted an indispensable component of a multitude of optical systems, such as in laser tracker systems to guarantee accurate distance measurements [1] and in Michelson interferometers to augment measurement precision [2]. In the aerospace field, satellites use retroreflectors to maintain or determine distances during orbital maneuvers. Recently, the demand for in-situ evaluation of the reflective properties of retroreflectors has grown, particularly in thermonuclear fusion applications, where such techniques have become indispensable for calibrating the sensitivity of spectroscopic measurements in optical diagnostics.

In optical plasma diagnostics of fusion reactors, plasma emission is relayed through a series of optical components (mirrors, vacuum windows, fibers, and spectrometers) to a photodetector [3–6]. To convert the electrical signal of the photodetector into a physically meaningful parameter, such as spectral radiance, absolute sensitivity calibration is essential, which entails an analysis of the intensity ratio between transmitted light and light with known fundamental characteristics incident on the optical system. However, using a standard light source inside the vacuum vessel is impractical in the context of the international thermonuclear experimental reactor (ITER) due to port constraints and concerns about material property changes induced by radiation. Thus, an alternative methodology was proposed whereby the transmittance of an optical system could be inferred by using light from outside the vacuum vessel that is reflected via a retroreflector temporarily installed at the tip of the optical system [7]. In particular, the retroreflector, which is mounted on a shutter between the plasma and a plasma-facing mirror, enters the optical

* Corresponding author.
E-mail address: natsume.hiroki.l@tokai.ac.jp (H. Natsume).

https://doi.org/10.1016/j.ijleo.2025.172350
Received 3 December 2024; Received in revised form 31 March 2025; Accepted 9 April 2025
Available online 26 April 2025
0030-4026/© 2025 The Authors. Published by Elsevier GmbH. This is an open access article under the CC BY-NC-ND license (http://creativecommons.org/licenses/by-nc-nd/4.0/).

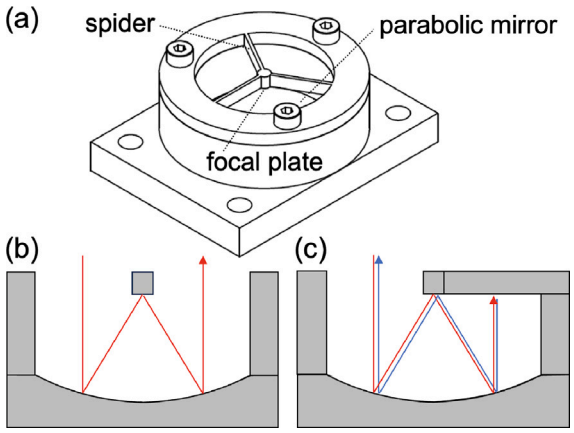

Fig. 1. (a) Schematic of our cat's eye. The optical path of (b) the three-time reflection and (c) the seven-time reflection.

path when the shutter is closed and is removed from the optical path upon opening. While this method appears straightforward, a critical challenge arises when the optical parameters of the system, such as transmittance and reflectance, change over time. This is particularly problematic when using conventional corner-cube retroreflectors or Luneburg lenses, which do not allow for independent characterization of their reflectance.

In ITER's optical diagnostics, several environmental factors contribute to changes in optical properties—impurity deposition on mirrors facing the plasma; observed changes in mirror morphology [8]; attenuation of lens material [9] and fiber transmittance [10] due to gamma-ray irradiation; and solarization caused by high-energy ultraviolet photons. Therefore, variation in transmittance of the optics is a very real possibility. Even though some mirrors are cleaned of impurities by means of plasma sputtering, it cannot be guaranteed that the mirrors will perfectly regain their initial reflectance levels after repeated plasma sputtering [11–13]. Accordingly, it is imperative to conduct frequent sensitivity calibrations. However, retroreflectors are also susceptible to degradation in reflectance due to deposition of impurities and corrosion of mirror surfaces. Furthermore, the retroreflectors for some diagnostics in ITER, such as the divertor impurity monitor [14], cannot be cleaned owing to physical constraints and therefore reflectance cannot be recovered. Without a clear understanding of reflectance, it becomes challenging to distinguish between the retroreflector's attenuation and the optical path's transmittance, which hinders accurate absolute sensitivity calibration. Currently, no method has been established to determine the reflectance of a retroreflector located in the radiation environment of the vacuum vessel, which is inaccessible to humans. This challenge significantly restricts the feasibility of using retroreflectors for absolute sensitivity calibration in the ITER environment.

This study presents a method for the in-situ measurement of the reflectance of a cat's-eye retroreflector situated at the tip of an optical system. Unlike conventional retroreflectors, the geometry of a cat's-eye retroreflector mirror allows for reflectance to be determined independently by exploiting the variations in number of reflections and reflection positions. Likewise, this method allows for in-situ measurement of transmittance in optical systems in a vacuum, thereby enabling absolute sensitivity calibration. This method was verified through optical ray-tracing simulations and actual physical experiments. Section 2 explains the underlying principle, Section 3 presents the simulation results, Section 4 provides experimental methods and results, while a discussions is given in Section 5, and Section 6 is the conclusion.

2. Principle

Fig. 1(a) depicts an isometric view of the cat's-eye retroreflector (hereafter referred to as cat's eye) used in this study. An exploded view is provided in Fig. A1 in the Appendix. The cat's eye is composed of a parabolic mirror, a focal plate, and a 3-vane spider. The focal plate is positioned at the focal point of the parabolic mirror and is supported by the spider, which has a reflective mirror surface. The term spider here is analgous to the spiders of telescopes, meaning a structural component that supports elements at the focal point. Fig. 1(b) illustrates the light path in a typical cat's eye. The light incident on the parabolic curve is reflected in a three-stage process: initially towards the focal plate, then from the focal plate to the parabolic mirror, and finally from the parabolic mirror back towards the light source. The spider acts as a support to hold the focal plate in the correct position and angle, and is designed to be as thin as possible to avoid obstructing the path of the emitted light. In contrast to typical designs, we actively use the spider to capitalize on reflected light having a different optical path and number of reflections, as illustrated in Fig. 1(c). The light incident on the cat's eye is initially reflected by the parabola, then by the focal plate, and subsequently by the parabola once more, directing it towards the direction of the light source. The light is then further reflected by the spider, returning along the light path from which it came for a total of seven reflections along its optical path.

The radiant flux for the recursive light of the three-time reflection ($\Phi_3(r,\theta)$) and the seven-time reflection ($\Phi_7(r,\theta)$) is expressed by Eqs. (1) and (2), respectively:

$$\Phi_3(r,\theta) = R^3(r,\theta)\,T^2(r,\theta)\,T_{\mathrm{bs}}\left(1-T_{\mathrm{bs}}\right)\Phi_{\mathrm{i}}, \tag{1}$$

$$\Phi_7(r,\theta) = R^7(r,\theta)\,T^2(r,\theta)\,T_{\mathrm{bs}}\left(1-T_{\mathrm{bs}}\right)\Phi_{\mathrm{i}}, \tag{2}$$

where r represents the radius from the center of the cat's eye, θ is the polar angle, R is the reflectance of one surface of the cat's eye, T is the transmittance of an optical path without the cat's eye, and Φ_{i} is the radiant flux of the light source. T_{bs} denotes the transmittance of a beamsplitter used to measure radiant flux, introduced later in this paper. Assuming that $R\left(r,\theta_3\right) = R\left(r,\theta_7\right)$ and $T\left(r,\theta_3\right) = T\left(r,\theta_7\right)$, where θ_3 and θ_7 are the polar angles for the three- and seven-time reflections, respectively, the ratio of Eq. (1) to Eq. (2) yields an R expression solely in terms of Φ_3 and Φ_7 as follows:

$$R\left(r,\theta_3\right) = \left(\frac{\Phi_7\left(r,\theta_7\right)}{\Phi_3\left(r,\theta_3\right)}\right)^{1/4}. \tag{3}$$

Finally, by substituting Eq. (3) for R in Eq. (1), T can be determined as follows:

$$T\left(r,\theta_3\right) = \left(\frac{\Phi_3\left(r,\theta_3\right)}{\Phi_{\mathrm{i}}R^3\left(r,\theta_3\right)T_{\mathrm{bs}}\left(1-T_{\mathrm{bs}}\right)}\right)^{1/2}. \tag{4}$$

3. Simulations

Ray-tracing simulations were performed using the ray-tracer Raysect [15], the setup of which is illustrated in Fig. 2(a). The reflectance of each mirror in the cat's eye was set at 51%. The intermediate optical system in front of the cat's eye consisted solely of a mirror having a reflectance of 92%. Thus, the overall transmittance of the system was also 92%. Note that the reflectance of the cat's eye and the transmittance of the system are regarded as unknown variables and are the targets for estimation. The beamsplitter's transmittance was fixed at a known value of 50%. The cat's eye object data, consistent with that depicted in Fig. 1(a), was imported into the ray-tracer as three-dimensional CAD data. The radius of the cat's eye was 10 mm. The parabolic curve of the parabolic mirror is described by the equation $y = x^2/40$, where the y-axis runs parallel to the direction of incident light, and the x-axis is perpendicular to it. The focal point is located at $y = 10$ mm. Upon injection of collimated light, the observed pattern on the detector can be seen in Fig. 2(b). Two sets of three lines emanate from the center, positioned opposite each other with respect to the center. The three lines having straight edges are from reflections on the source side, while the remaining set of three lines having jagged edges represent the recursive light of the seven-time reflection. Recursive light resulting from the three-time reflection is observed between the radial lines.

The absence of complete smoothness in the 3D CAD model's surface resulted in noticeable discontinuities in the simulation results. Consequently, we calculated the average values of Φ_3 and Φ_7 for the variable r, which were found to be 0.0262 a.u. and 0.00153 a.u., respectively. Using Eq. (3), the reflectance R was determined to be 49%. With the transmittance of the beamsplitter set at 50%, the transmittance of the intermediate optical system was calculated to be 94%. Despite minor discrepancies due to rounding errors, the reflectance of the cat's eye and the transmittance of the intermediate optical system were effectively obtained.

4. Experimental verification

Physical experiments were conducted to validate the results of the simulations. A schematic of the experimental setup is illustrated in Fig. 3(a). An expanded laser diode beam with a radius of 1 cm was directed through a beamsplitter and was then reflected twice by two mirrors onto the cat's eye. The two mirrors were carefully adjusted to ensure that the light was incident on the cat's eye perpendicularly. The reflective surface of the cat's eye was coated with a layer of molybdenum. The recursive light emitted from the cat's eye was subsequently directed through a lens and captured by an imaging sensor. A beamsplitter having a transmittance of 90% and a reflectance of 10% was used. The primary objective was to estimate the reflectance of the cat's eye and subsequently determine the combined transmittance of the two mirrors. To validate the results, reflectances at the focal plate of the cat's eye and the two mirrors were measured using a spectrophotometer (JASCO Corp.: V-750).

Due to the laser beam not being perfectly parallel, the light reflected seven times was overlapped by the light reflected three times. Accordingly, based on the obtained image shown in Fig. A2 in the Appendix, the R value at a wavelength of 650 nm was calculated to be 70%, which is a notable discrepancy from the spectrophotometer's measured value of 57.8%. To address this issue, the spider was covered with carbon tape, as depicted in Fig. 3(b), to ensure that the light from the three-time reflection did not overlap with the light from the seven-time reflection. An image acquired with the spider covered in carbon tape is shown in Fig. 3(c), wherein the three-time reflection and seven-time reflections are distinctly discernible. The value of R was found to be 56.5%, which aligns with the spectrophotometer measurement. Furthermore, the value of R was determined by using a variety of laser diodes, each with a distinct wavelength. The R values and those measured by the spectrophotometer are plotted as a function of wavelength in Fig. 4. At 405 nm and 532 nm, the results were also found to be consistent with the spectrophotometer values. Using the determined R, the transmittance T of the optical path, which is the product of the reflectances of the two mirrors, can be derived using Eq. (4). The computed values and spectrophotometer measurements are plotted in Fig. 4. The computed T was calculated to be 71.0% at 650 nm and was comparable to the spectrophotometer value of 69.8%. Similarly, the results at 405 and 532 nm were also consistent with the spectrophotometer measurements.

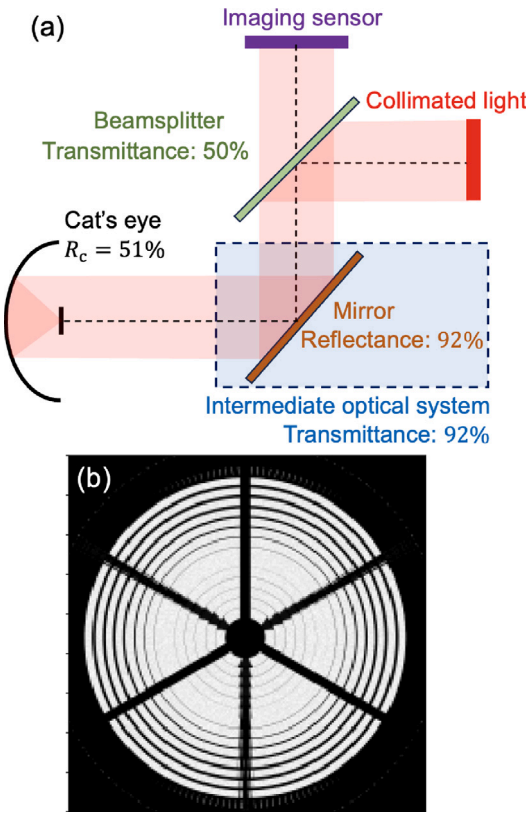

Fig. 2. (a) Schematic of the ray-tracing simulation setup, and (b) a rendered image captured on the imaging sensor.

5. Discussion

According to Fresnel's law, the reflectance varies depending on the angle of incidence. Nevertheless, this relationship is neglected in Eqs. (1)–(4). In this section, we will examine the impact of incorporating or excluding Fresnel's equations in our analysis. The angle of reflection on a parabolic mirror, denoted as ψ_1, is the angle between the normal to the tangent line of $y = x^2/40$ and $x = r$; it is expressed as follows:

$$\psi_1(r) = \arctan\frac{r}{20}. \tag{5}$$

The reflected light originates from $(y, x) = \left(r, r^2/40\right)$ mm and is directed towards the focal plate located at $(y, x) = (0, 10)$ mm. The incident angle of this reflection on the focal plate, denoted as ψ_2, can be defined as follows:

$$\psi_2(r) = \arctan\frac{r}{10 - r^2/40}. \tag{6}$$

As r increases, both ψ_1 and ψ_2 increase monotonically, reaching values of 27° and 53° at $r = 10$ mm, respectively. Re-expressing Eqs. (1)–(2) in terms of ψ_1 and ϕ_2, we obtain the following relation:

$$\Phi_3 = R^2\left(\psi_1(r)\right) R\left(\psi_2(r)\right) T^2 T_{\mathrm{bs}}\left(1 - T_{\mathrm{bs}}\right)\Phi_{\mathrm{i}}, \tag{7}$$

$$\Phi_7 = R^4\left(\psi_1(r)\right) R^2\left(\psi_2(r)\right) R\left(\psi = 90°\right) \times T^2 T_{\mathrm{bs}}\left(1 - T_{\mathrm{bs}}\right)\Phi_{\mathrm{i}}, \tag{8}$$

wherein θ is omitted for the sake of simplicity. The parameters $\alpha(r)$ and $\beta(r)$ represent the ratio of reflectance when the incident light is perpendicular to the reflective surface (i.e., when $\psi_1 = 0$ and $\psi_2 = 0$) relative to the reflectance at a non-zero angle of incidence. Given these definitions, the ratio of Eq. (7) to Eq. (8) is expressed as:

$$\left(\alpha^2(r)\,\beta(r)\right)^{1/4} R\left(0°\right) = \left(\frac{\Phi_7}{\Phi_3}\right)^{1/4}. \tag{9}$$

Namely, the variation due to the incident angles can be represented as a function of $\left(\alpha^2(r)\,\beta(r)\right)^{1/4}$ when estimating R. In addition, the influence on T is proportional to $\left(\alpha^2(r)\,\beta(r)\right)^{-3/8}$, as described by Eq. (4). Fig. 5 shows $\left(\alpha^2(r)\,\beta(r)\right)^{-3/8}$ for mirrors

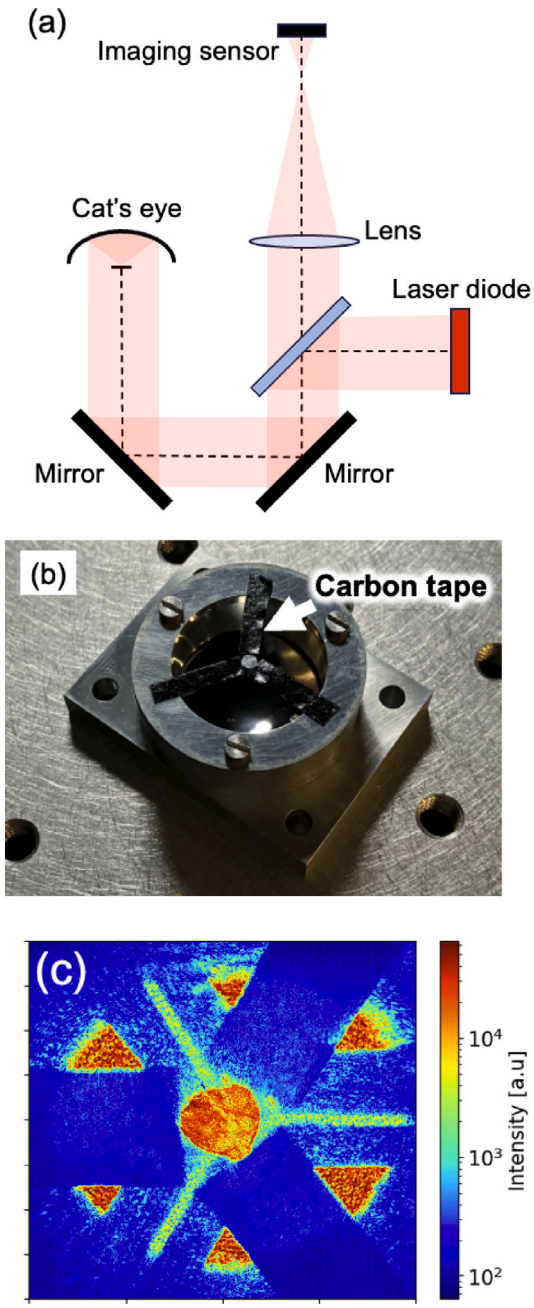

Fig. 3. (a) Schematic of the experimental setup. (b) Photograph of the cat's eye with carbon tape applied to the spider. (c) Image obtained and displayed on the imaging sensor.

made of silver (Ag), aluminum (Al), titanium (Ti), rhodium (Rh), tungsten (W), and molybdenum (Mo) when plotted against r at a wavelength of 650 nm. Note that the optical constants for Ag, Al, Ti, and W were based on [16], and those for Mo and Rh were based on [17]. All metals exhibited values exceeding $\sim 99.0\%$ within $r = 10$ mm, and the variation arising from treating the angle of incidence as vertical versus considering the angle of incidence precisely was less than approximately 1%. Therefore, we can infer that accurate consideration of the angle of incidence is not particularly sensitive to T in this cat's eye design. A notable discrepancy is observed when comparing different metals, in particular with Mo, but this discrepancy can be effectively mitigated by using metals such as Ag or Al. Additionally, in consideration of the impact of thermal load in a fusion reactor, high melting point materials such as Ti, Rh, and W are preferable. Among these, Rh displays the highest resistance and appears to be the most suitable.

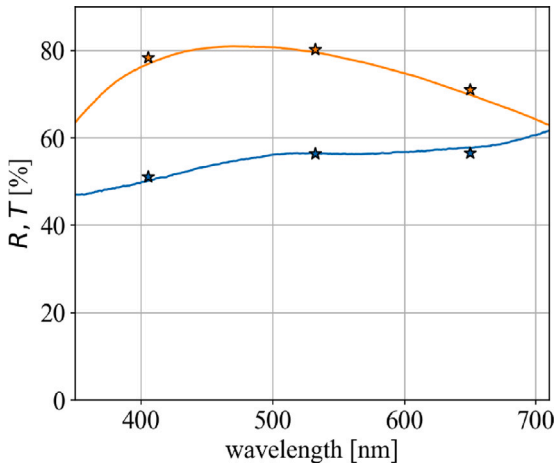

Fig. 4. Reflectance R (blue) and transmittance T (orange) as a function of wavelength: Spectrophotometer measurements (solid line) and values computed using Eq. (3) or (4) (star mark).

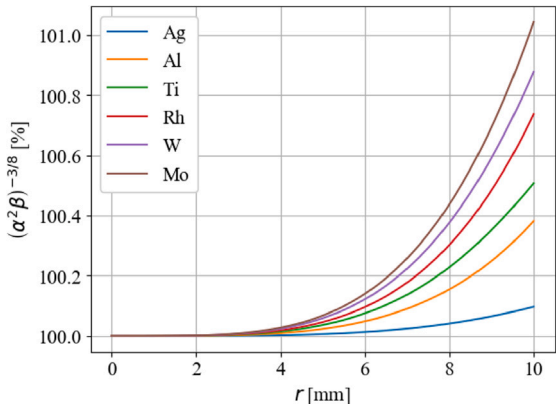

Fig. 5. Variation in reflectance when treating the angle of incidence as vertical versus considering the exact angle of incidence for mirrors made of various metals.

6. Conclusion

In this study, we observed that a cat's-eye retroreflector produces two types of reflected light, which are distinguished by their reflection positions and the number of reflections. We found that the intensity ratio between these two reflections is exclusively determined by the reflectance of the cat's eye and is independent of the transmittance of an optical system when the cat's eye is excluded. This discovery facilitates the precise identification of the reflectance of the cat's eye and, subsequently, the transmittance of the optical system when the cat's eye is excluded.

A cat's-eye retroreflector functions optimally when the incident light is directed towards the focal point of its parabolic mirror. If the incident angle deviates significantly, the light will not properly focus, disrupting the retroreflection process. However, minor deviations can be mitigated by slightly increasing the size of the focal plate. Moreover, in our experiment, we applied carbon tape to the spider structure to prevent overlap between different reflection paths. Alternatively, modifying the spider structure by increasing its width and chamfering its edges could eliminate the need for additional masking materials. Furthermore, in our experiment, we demonstrated that incorporating two mirrors between the light source and the cat's eye and adjusting their angles enabled the light from the source to be incident on the cat's eye perpendicularly with sufficient accuracy.

The effectiveness of this principle in calibrating the transmittance of an optical system was validated through both simulations and experiments. Furthermore, the method remains largely unaffected by variations in reflectance due to changes in incidence angles, a phenomenon described by Fresnel's law. Specifically, mirrors made of rhodium have high reflectivity and appear to be suited for environments with high thermal loads.

In conclusion, our proposed method offers a solution for the expansive calibration needs of ITER optical systems. Our method is not limited to use in ITER but could also be used for other applications, e.g., measuring the transmittance of a vacuum window without opening the vessel to the atmosphere when performing emission spectroscopy in laboratory and process equipment.

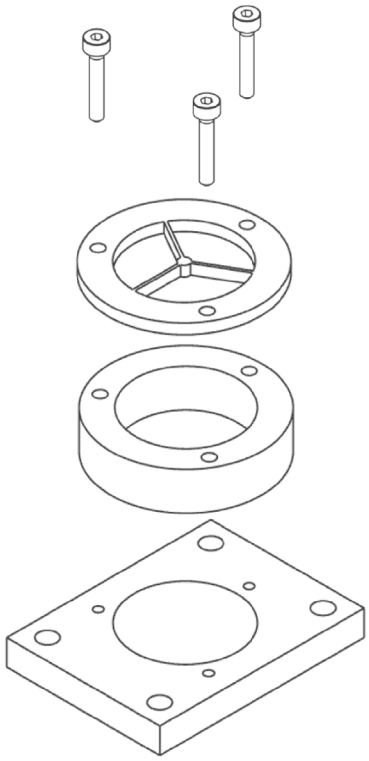

Fig. A1. Exploded view of our cat's eye.

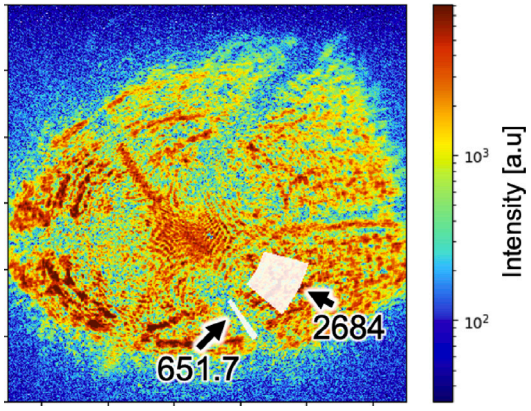

Fig. A2. Image captured on the imaging sensor without carbon tape applied to the spider.

CRediT authorship contribution statement

Hiroki Natsume: Writing – original draft, Visualization, Software, Methodology, Investigation, Formal analysis, Conceptualization. **Sin-iti Kitazawa:** Writing – review & editing, Methodology. **Kunpei Nojiri:** Validation. **Kazuhiro Torimoto:** Methodology. **Eiichi Yatsuka:** Resources, Formal analysis. **Tomohiro Yokozuka:** Software. **Takanori Kikuchi:** Investigation. **Yoshihiko Nunoya:** Resources, Project administration.

Declaration of competing interest

The authors declare the following financial interests/personal relationships which may be considered as potential competing interests: Has patent pending to. If there are other authors, they declare that they have no known competing financial interests or personal relationships that could have appeared to influence the work reported in this paper

Appendix

See Figs. A1 and A2.

Data availability

Data will be made available on request.

References

[1] S. Shao, et al., IEEE INFOCOM 2018 - IEEE Conference on Computer Communications, IEEE, 2018.
[2] P. Haschberger, et al., Appl. Opt. 29 (28) (1990) 4216.
[3] T. Sugie, et al., Rev. Sci. Instrum. 70 (1) (1999) 351–354.
[4] H. Ogawa, et al., Fusion Eng. Des. 83 (10–12) (2008) 1405–1409.
[5] B.L. Linehan, et al., Rev. Sci. Instrum. 89 (10) (2018).
[6] C. Pastorand others, Fusion Eng. Des. 168 (2021) 112607.
[7] T. Takemoto, et al., Optik 127 (5) (2016) 2950–2953.
[8] S. Kajita, et al., J. Instrum. 15 (11) (2020) P11035–P11035.
[9] S. Kitazawa, et al., Plasma Fusion Res. 14 (2019) 3405089–3405089.
[10] A.T. Ramsey, et al., Rev. Sci. Instrum. 68 (1) (1997) 632–635.
[11] A.V. Rogov, et al., Instruments Exp. Tech. 58 (1) (2015) 161–166.
[12] J. Peng, et al., Plasma Sci. Technol. 22 (3) (2019) 034004.
[13] F. Sanchez, et al., J. Nucl. Mater. 581 (2023) 154382.
[14] H. Ogawa, et al., Plasma Fusion Res. 2 (2007) S1054–S1054.
[15] A. Meakins, et al., Raysect Python raytracing package, Zenodo v0.8.1 (2023).
[16] A.D. Rakić, et al., Appl. Opt. 37 (22) (1998) 5271.
[17] Filmetrics Refractive Index Database, Available from http://www.filmetrics.com/refractive-index-database/, 2023.